RAA 2018 Vol. **18** No. **9**, 107(10pp) doi: 10.1088/1674–4527/18/9/107

http://www.raa-journal.org *http://iopscience.iop.org/raa*

***R**esearch in*
***A**stronomy and*
***A**strophysics*

Upgraded photometric system on the 85-cm telescope at Xinglong station

Chun-Hai Bai[1,2,3], Jian-Ning Fu[4], Tao-Ran Li[1], Zhou Fan[1], Jiang-Hua Wu[4], Yong Zhao[1], Xian-Qun Zeng[1], Wen-Zhao Zhang[4], Peng Qiu[1], Guo-Jie Feng[3] and Xiao-Jun Jiang[1]

[1] National Astronomical Observatories, Chinese Academy of Sciences, Beijing 100101, China; *baichunhai@xao.ac.cn*
[2] University of Chinese Academy of Sciences, Beijing 100049, China
[3] Xinjiang Astronomical Observatory, Chinese Academy of Sciences, Urumqi 830011, China
[4] Department of Astronomy, Beijing Normal University, Beijing 100875, China

Received 2017 May 30; accepted 2018 April 12

Abstract The 85-cm telescope at Xinglong station is a prime focus system that operates well with high science outputs. The telescope has been upgraded since 2014 with a new corrector, and new filters and camera, which are provided by Beijing Normal University. The filter set is the Johnson-Cousins $UBVRI$ system. We report the test results of the new system including bias, dark current, linearity, gain and readout noise of the CCD camera. Then we derive accurate instrumental calibration coefficients in $UBVRI$ bands with Landolt standard stars during photometric nights. Finally, we give the limiting magnitudes with various exposure times and signal-to-noise ratios for observers as references.

Key words: telescope — instrumentation — CCD photometry

1 INTRODUCTION

The 85-cm telescope is located at Xinglong station (117°34′ 39″ East, 40°23′ 26″ North; at an altitude of about 960 m) of National Astronomical Observatories, Chinese Academy of Sciences (NAOC). This telescope is jointly operated by Beijing Normal University and NAOC (Fan et al. 2016). The seeing values during 80% of nights are below $2.6''$ with the distribution peak around $1.8''$. The sky brightness at zenith is around 21.1 mag arcsec^{-2} in the V-band. The average number of observable nights is 230 per year and the average fraction of photometric nights is 32% (Zhang et al. 2015a, 2016). The main scientific projects include multi-color photometry of pulsating stars (Luo et al. 2012), binaries (Yang 2013; Zhang et al. 2015c,b), exoplanets (Zhang & Pi 2015) and variable stars (Zhang et al. 2012).

From 2014 to 2015, the telescope was upgraded by local technicians. It would be quite helpful and important if observers could get to know the properties and performance of the telescope, including the bias, dark current and linearity of the CCD. In addition, analyzed results of the CCD photometric system are reported, such as the throughput, detection limit and instrument response.

We introduce the 85-cm observation system in Section 2. Then the CCD characteristics are reported in Section 3. The photometric calibration and transformation coefficients are provided in Section 4. The throughput and detection limit are addressed in Section 5, and a summary is given in Section 6.

2 OBSERVATION SYSTEM

The 85-cm telescope is mounted equatorially. The effective diameter of the parabolic primary mirror is 850 mm, concentrating 80% of the energy into a circle with diameter of $1.6''$. The original focal length was 3000 ± 150 mm. With the new corrector, the focal ratio of the prime focus reduced from 3.75 to 3.5. The new CCD camera is an Andor iKon back-illuminated DZ936N-BV with 16 bit A/D converter. It is scientific-grade without an anti-blooming gate, which was purchased by the Department of Astronomy, Beijing Normal University and was mounted to the telescope in Oct. of 2014.

The specifications in the product manual are listed in Table 1. It has a 5-stage Peltier cooling system which can reach $-80°$C by air cooling or $-95°$C by coolant with a recirculator. With a 2048×2048 imaging array ($13.5 \times 13.5\,\mu$m pixel^{-1}), the field of view of the CCD is $32' \times 32'$, which is four times the size of the original $16.5' \times 16.5'$ (Zhou et al. 2009), and the pixel scale of $0.93''$ is similar to what was formerly reported. A Johnson-Cousins standard *UBVRI* filter system made by FLI started to serve in observations since Sep. of 2015. Time synchronization can be realized through the onsite networks whenever needed.

3 CCD CHARACTERISTICS

3.1 Bias Level

The bias level of the chip was tested at the CCD temperature of $-70°$C. We took the bias images during the night of 2017 Oct. 11. During the test, the ambient temperature changed from $3°$C to $6°$C as shown in Figure 1. One can see that the bias is very stable with a mean value of about 300 ± 2 analog-to-digital unit (ADU). The scan rate of the chip was set to 1 MHz with a gain of $1\times$. Table 2 lists the test results.

3.2 Gain and Readout Noise

The gain G is the factor describing how the digital output is converted to the number of electrons, which is useful for evaluating the performance of the CCD camera. We measured the gain by comparing the signal level to the amount of variation in the flat field and bias images. The gain and readout noise can be measured by Equations (1) and (2) (Howell 2000; Jones 2006) with Image Reduction and Analysis Facility's (IRAF's, provided and maintained by NOAO) task *findgain*. The task *findgain* uses these equations to calculate the gain and readout noise with two dome flats and two bias frames. When we select CCD gain $4\times$ and scan rate 1 MHz which are used by most observers, the test values of gain and readout noise are $0.97\,e^-$/ADU and $6.8\,e^-$ respectively. These results approach the values provided by the product manual of $1\,e^-$/ADU and $7.0\,e^-$, respectively, as listed in Table 1.

$$\text{Gain} = \frac{(\overline{F1}+\overline{F2})-(\overline{B1}+\overline{B2})}{\sigma^2_{F1-F2}-\sigma^2_{B1-B2}}\,, \quad (1)$$

$$\text{Readout noise} = \frac{\text{Gain}\cdot\sigma_{\overline{B1}-\overline{B2}}}{\sqrt{2}}\,. \quad (2)$$

3.3 Dark Current

The dark current measurement was recorded for one whole night on 2016 Apr. 14. The dark counts with 1200 s of exposure time were stable in columns and lines as shown in Figure 2. The dark images were taken with exposure times from 100 s to 1800 s. For each exposure time, two frames were acquired. Hence, we calculated the mean and standard deviation for each image. As shown in Figure 3, the measured dark current is $0.00448 \pm 0.00027\,e^-$ pixel^{-1} s^{-1}. This value seems to be much larger than that given in the product manual ($0.00040\,e^-$ pixel^{-1} s^{-1} @ $-70°$C), but the impact on practical observation is very small. Therefore, dark correction is unnecessary for an exposure which is shorter than 600 s.

3.4 Linearity

The linearity of a CCD is important for high precision photometry. In order to check linearity of the response in the CCD, we carried out measurements with dome flats over two nights in May 2016. As the amount of stray light changes with the Sun during daytime, the measurements were taken after dusk. We closed the shutter and adjusted the dome light by attaching several pieces of A4 paper to the dome, which made it dim enough for the CCD camera to take long exposures.

At the beginning, we set different CCD exposure times to make the ADU values larger than 60 000, far from saturated with gain $4\times$ and scan rate 1 MHz. The ADU values became smaller when we changed the gain setting to $2\times$ and $1\times$. We could calculate the values through the acquired images, which were corrected for bias, as listed in Table 3.

Then, we pointed the telescope near the zenith and carried out two groups of linearity measurements with the dome light. For each exposure time, we took six frames. The mean ADU values for a 400×400 region close to the CCD center were counted. For one group with CCD scan rate of 1 MHz and gain of $1\times$, we set the exposures from 0.1 s to 70 s. The mean count increased with the exposure time, but the standard deviation dropped after the CCD reached its full well. The peak in linearity with gain $1\times$ was larger than 29 000, as shown in Figure 4, which multiplied by the gain value of 3.43 equals 99 470 (>99 000). One can find that the linearity is better than 99% for the full well. For another group with scan rate 1 MHz and gain $4\times$, the exposure

Table 1 Specifications of the CCD Camera According to the Product Manual

Features	Specifications
Pixel number	2048×2048
Pixel size	$13.5\,\mu\mathrm{m} \times 13.5\,\mu\mathrm{m}$
Imaging area	$27.6\,\mathrm{mm} \times 27.6\,\mathrm{mm}$
Fill factor	100%
A/D conversion	16 bit
Full well	100 000 e^-
Scan rate	50 kHz, 1 MHz, 3 MHz, 5 MHz (visualization mode)
Full frame readout time	91 s@50 kHz, 4.5 s@1 MHz, 1.65 s@3 MHz, 1.05 s@5 MHz
Operating temperature	-80°C Air cooled, -95°C Coolant recirculator
	-100°C Coolant chiller, coolant @ 10°C, 0.75 l/min
Readout noise	2.9e^- @ 50 kHz, 7.0e^- @ 1 MHz,
	11.7e^- @ 3 MHz, 31.5e^- @ 5 MHz
Dark current ($\mathrm{e}^-\,\mathrm{pixel}^{-1}\,\mathrm{s}^{-1}$)	0.00040 @ -70°C, 0.00013 @ -80°C, 0.000059 @ -100°C
Linearity	> 99 %

Table 2 Test Results about Bias, Gain, Readout Noise, Dark Current and Linearity

Bias (ADU)	Mean value 300±3 @ 1 MHz, Gain 1×
Gain	0.97 @ 1×, 1.88 @ 2×, 3.43 @ 4×, @ 1 MHz
Readout noise	6.8e^- @ 1 MHz, Gain 1×
Dark current (e^- pixel^{-1} s^{-1})	0.00448±0.00027 @ -70°C
Linearity	$> 99.6\%$

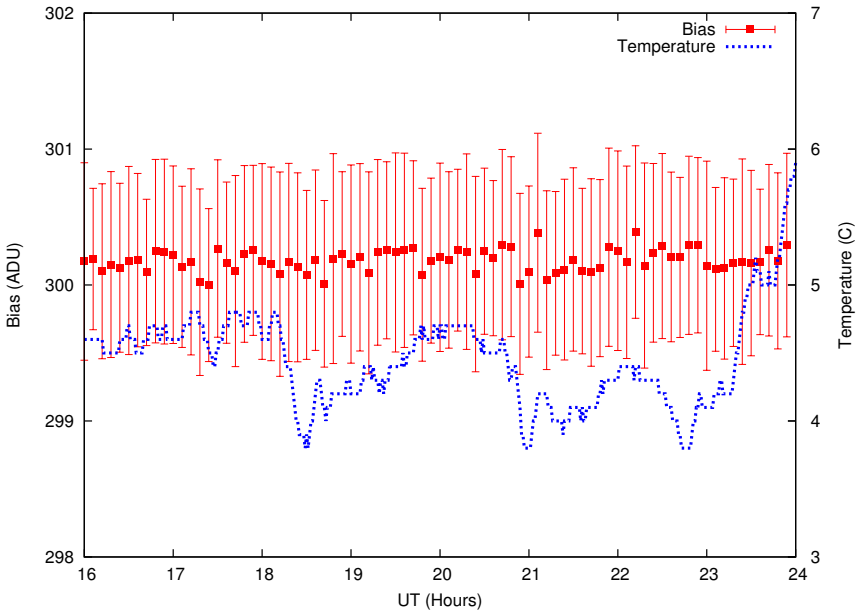

Fig. 1 Bias level at the temperature of -70°C, with a scan rate of 1 MHz and gain of 4×. The *blue curve* shows the temperature variations.

time was set from 0.5 s to 46 s. When the gain was 4× (real value is 0.97), the 16 bit ADU value decreases after the A/D converter saturated at 65 535 as shown in Figure 5. We understand that the electron count is far from the full well of 100 000. At the low edges of the data points in the two figures, the mean value deviated from the fit line, which is due to the shutter effect. Therefore, we suggest an exposure time larger than 3 s.

4 PHOTOMETRIC CALIBRATION

The magnitudes measured from the images are the telescope instrumental magnitudes. In order to compare the

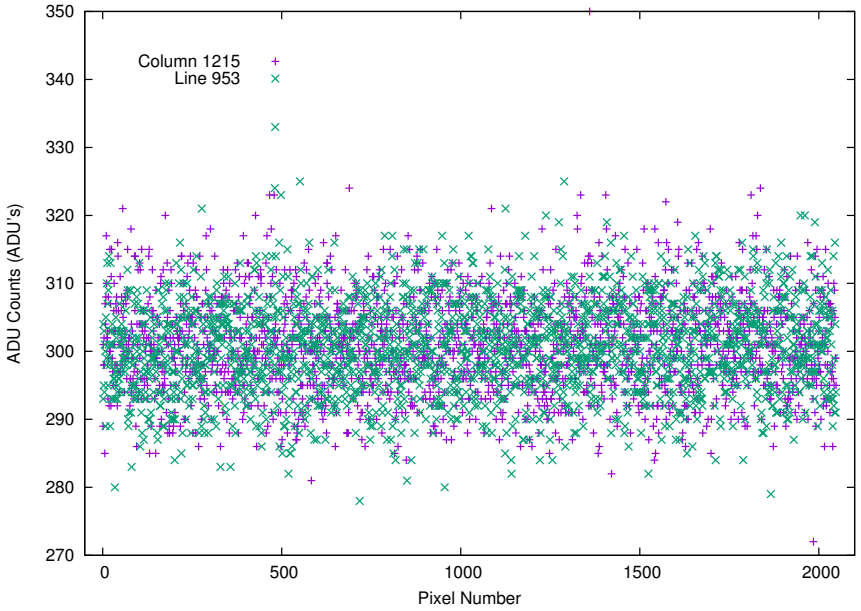

Fig. 2 ADU distribution of a 1200 s dark image at the CCD temperature of -70°C, with scan rate of 1 MHz in arbitrary column and line.

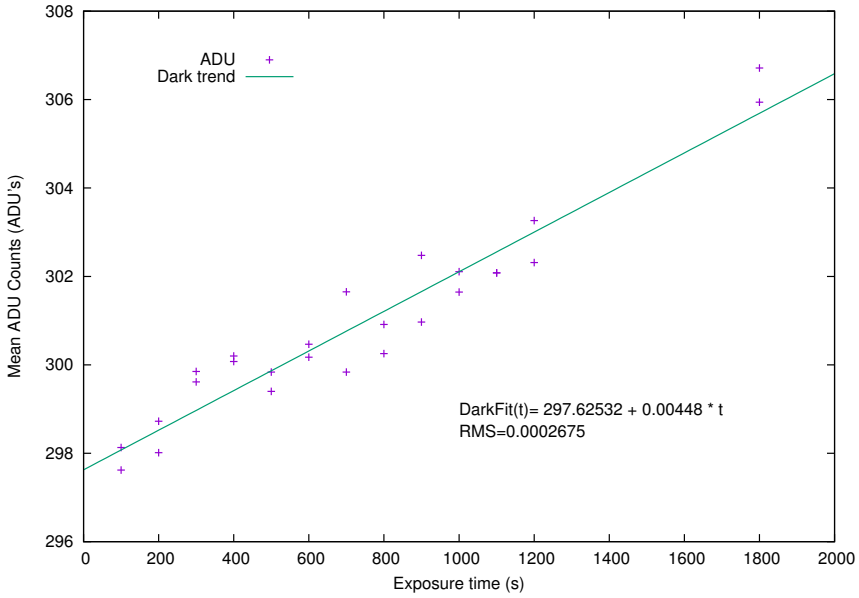

Fig. 3 The average ADU count versus exposure time for dark images. The solid line is the best linear fit between the average ADU count and exposure time.

photometric result with that from other instruments, one needs to calibrate the magnitudes from the instrumental system into the standard system. In Feb., Mar. and Apr. 2016, we selected some stars from Landolt standards (Landolt 1992, 2013) as listed in Table 4, considering both the magnitude and colors. Some of them can pass the zenith at Xinglong station and, hence, are suitable for calibration.

Table 3 Gain Values with Scan Rate @ 1 MHz

Exposure time	Gain selected	Mean ADU	Gain value
30 s	1×	18284	3.43
30 s	2×	33468	1.88
30 s	4×	62863	0.97

The seeing values approximated $2.2''$ during the observation night. After collecting photometric data on the standard stars, all frames were reduced with 2 times the

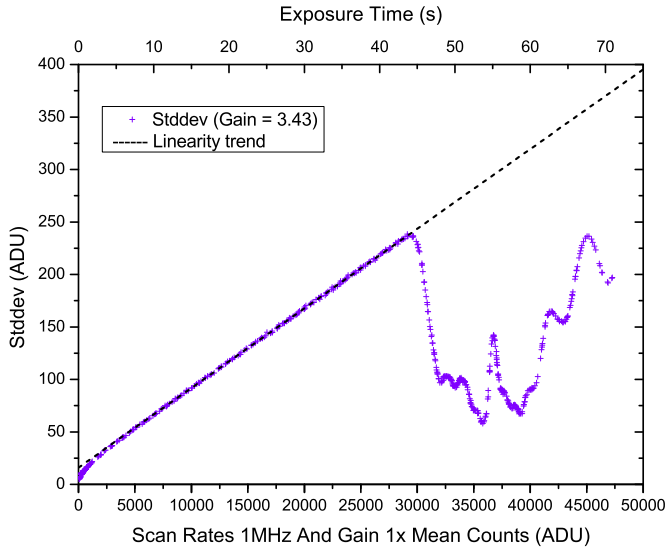

Fig. 4 Plot of the standard deviation versus mean count of the dome flat with a CCD scan rate of 1 MHz and gain 1×.

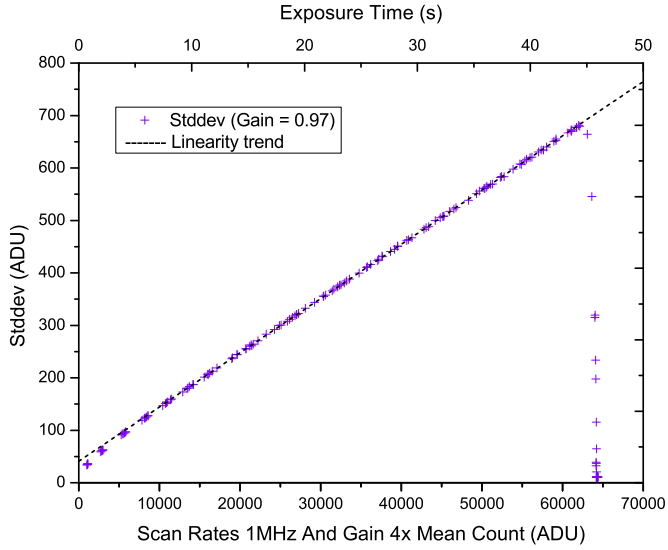

Fig. 5 Plot of the standard deviation versus the mean count of the dome flat with CCD scan rate of 1 MHz and gain 4×.

aperture by standard photometry steps using the *apphot* package in IRAF. We take 25 as our instrumental magnitude zero point, then the instrumental magnitudes and airmass are obtained. We define transformation equations offered by IRAF as follows:

$$U_{\rm inst} = U_{\rm std} + Z_U + K_U^{'}X + C_U(U-B)_{\rm std}\,, \quad (3)$$

$$B_{\rm inst} = B_{\rm std} + Z_B + K_B^{'}X + C_B(B-V)_{\rm std}\,, \quad (4)$$

$$V_{\rm inst} = V_{\rm std} + Z_V + K_V^{'}X + C_V(B-V)_{\rm std}\,, \quad (5)$$

$$R_{\rm inst} = R_{\rm std} + Z_R + K_R^{'}X + C_R(V-R)_{\rm std}\,, \quad (6)$$

$$I_{\rm inst} = I_{\rm std} + Z_I + K_I^{'}X + C_I(V-I)_{\rm std}\,, \quad (7)$$

where $U_{\rm std}$, $B_{\rm std}$, $V_{\rm std}$, $R_{\rm std}$ and $I_{\rm std}$ are the standard magnitudes, $U_{\rm inst}$, $B_{\rm inst}$, $V_{\rm inst}$, $R_{\rm inst}$ and $I_{\rm inst}$ are the instrumental magnitudes, Z_U, Z_B, Z_V, Z_R and Z_I are zero point magnitudes, $K_U^{'}$, $K_B^{'}$, $K_V^{'}$, $K_R^{'}$ and $K_I^{'}$ are the first-order extinction coefficients, C_U, C_B, C_V, C_R and C_I are the color terms in the transformation equations, and X denotes the airmass.

For each band we obtained 40 frames. Then, we used IRAF tasks *mknobsfile* and *fitparams* in the *photcal* package to fit the observed magnitudes and derive the coefficients. The extinction coefficients (K') and color terms (C) were fitted separately. The second-order extinction

Table 4 Landolt Standards used in 2016

Star Name	α (2000)	σ (2000)	V	$B-V$	$U-B$	$V-R$	$R-I$	$V-I$
104 456	12:42:53	–00:32:09	12.362	0.622	0.135	0.357	0.337	0.694
94 394	02:56:14	+00:35:25	12.273	0.545	–0.047	0.344	0.330	0.676
95 328	03:54:19	+00:36:47	13.525	1.532	1.298	0.908	0.868	1.776
97 75	05:57:55	–00:09:07	11.483	1.872	2.100	1.047	0.952	1.999
G44 27	10:36:02	+05:07:11	12.636	1.586	1.088	1.185	1.526	2.714
PG1047+3C	10:50:18	–00:00:21	12.453	0.607	–0.019	0.378	0.358	0.737
SA 29–322	09:46:31	+44:22:32	9.766	+0.488	+0.030	+0.285	+0.262	+0.560
SA 32–377	12:55:45	+44:40:38	10.630	+0.641	+0.101	+0.372	+0.358	+0.735
SA 35–343	15:51:57	+44:35:26	10.870	+0.433	–0.063	+0.271	+0.254	+0.529
SA 38–358	18:48:23	+45:23:22	9.854	+1.132	+1.186	+0.583	+0.509	+1.095
SA 29–324	09:46:53	+44:25:05	11.304	+1.117	+1.075	+0.582	+0.516	+1.097
SA 32–330	12:55:26	+44:33:35	10.068	+0.665	+0.190	+0.378	+0.342	+0.721
SA 35–339	15:51:54	+44:32:29	12.775	+0.554	+0.028	+0.336	+0.329	+0.662
SA 38–365	18:48:32	+45:25:10	11.625	+1.205	+1.309	+0.616	+0.546	+1.160

terms were too small to be ignored. The obtained transformation coefficients are listed in Table 5, including the filter names, zero points (Z), first-order extinction coefficients (K'), color terms (C) and root mean square (RMS) values. In Table 6, we compare our results with historical measurements at Xinglong station.

The comparison between Landolt standard magnitudes and calibrated magnitudes derived from the transformation equations in $UBVRI$ bands is shown in Figure 6.

With the relationship between Landolt standard magnitudes and shifted calibrated magnitudes using the transformation coefficients derived from observations taken in Feb., Mar. and Apr. 2016, the slopes of all the fitted lines are close to 1.0, so the calibration is good. The RMS of magnitude in each filter is smaller than 0.1 as listed in Table 6, indicating that the calibration relationship between the photometric system of the 85-cm telescope and the Johnson-Cousins standard photometric system is well established.

5 SYSTEM PERFORMANCE

5.1 System Throughput

The total throughput of the entire optical system can be estimated by observing a number of Landolt standards. The throughput includes the primary mirror reflection, correctors, filter response, quantum efficiency of the detector and atmospheric transformation. Kinoshita introduced his method (Kinoshita et al. 2005) and has worked at Lulin Observatory. We calculate the throughput efficiency of the 85-cm telescope in another way which was introduced by Fan et al. (Fan et al. 2016) based on the flux of Vega (Bohlin & Gilliland 2004; Bohlin 2014) following Equation (8).

$$\eta(\lambda) = \frac{F_{\rm ADU} \cdot {\rm G}}{F_\lambda \cdot \delta\lambda \cdot S_{\rm tel}}\,, \tag{8}$$

where $F_{\rm ADU}$ is the observed number of counts for a standard star per second (ADU s^{-1}); G is the gain of the CCD (e^{-1} ADU^{-1}); F_λ is theoretical photon flux of a standard star derived from its AB mag (photon s^{-1}cm^{-2} Å^{-1}); $\delta\lambda$ is the effective band width in the filter in imaging observations or the dispersion of the grating for spectroscopic observations (Å); $S_{\rm tel}$ is the effective area of the primary mirror of the telescope (cm^2) and λ is the effective wavelength of the filter or the wavelength at which the efficiency is computed for spectroscopy (Å).

The median throughputs in different bands are listed in Table 7.

5.2 Limiting Magnitude And Photometric Accuracy

The sky brightness has been introduced in detail by Zhang et al. (2015a), which is deeper than the detection limit for this 85-cm telescope. We can use Equation (9) to make an estimation (Howell 2000).

$${\rm SNR} = \frac{N_{\rm star}}{\sqrt{N_{\rm star} + n_{\rm pix}(N_{\rm sky} + N_{\rm dark} + N^2_{\rm readout})}}, \tag{9}$$

$$\sigma = 1.0857/{\rm SNR}\,, \tag{10}$$

where $N_{\rm star}$ is the total number of target photons collected by the CCD camera, $n_{\rm pix}$ the number of pixels which change with the seeing condition, $N_{\rm sky}$ the total number of photons on each pixel from sky background,

Table 5 Coefficients, Standard deviation and RMS of the 85-cm telescope photometric system

Filter	Zero point (Z)	Extinction (K')	Color Term (C)	RMS
$U_{\rm inst}$	4.732 ± 0.032	0.590 ± 0.022	–0.376 ± 0.034	0.051
$B_{\rm inst}$	1.781 ± 0.042	0.431 ± 0.029	–0.108 ± 0.011	0.043
$V_{\rm inst}$	1.909 ± 0.037	0.282 ± 0.026	–0.088 ± 0.025	0.052
$R_{\rm inst}$	1.977 ± 0.027	0.217 ± 0.019	–0.145 ± 0.008	0.049
$I_{\rm inst}$	2.383 ± 0.029	0.156 ± 0.021	–0.077 ± 0.008	0.050

Table 6 Extinction Coefficients at Xinglong Station

Year	K'_U	K'_B	K'_V	K'_R	K'_I	Reference
2016	0.590 ± 0.022	0.431 ± 0.029	0.282 ± 0.026	0.217 ± 0.019	0.156 ± 0.021	This paper
2011–2012		0.348±0.022	0.236±0.017	0.168±0.019	0.085±0.021	Huang et al. 2012
2008		0.330±0.007	0.242±0.005	0.195±0.004	0.066±0.003	Zhou et al. 2009
2006–2007		0.307±0.009	0.214±0.008	0.161±0.008	0.091±0.008	Huang et al. 2012
2004–2005		0.296±0.012	0.199±0.009	0.141±0.010	0.083±0.009	Huang et al. 2012
1995		0.35	0.20	0.18	0.16	Shi et al. 1998
1998		0.31	0.22	0.14	0.10	Shi et al. 1998

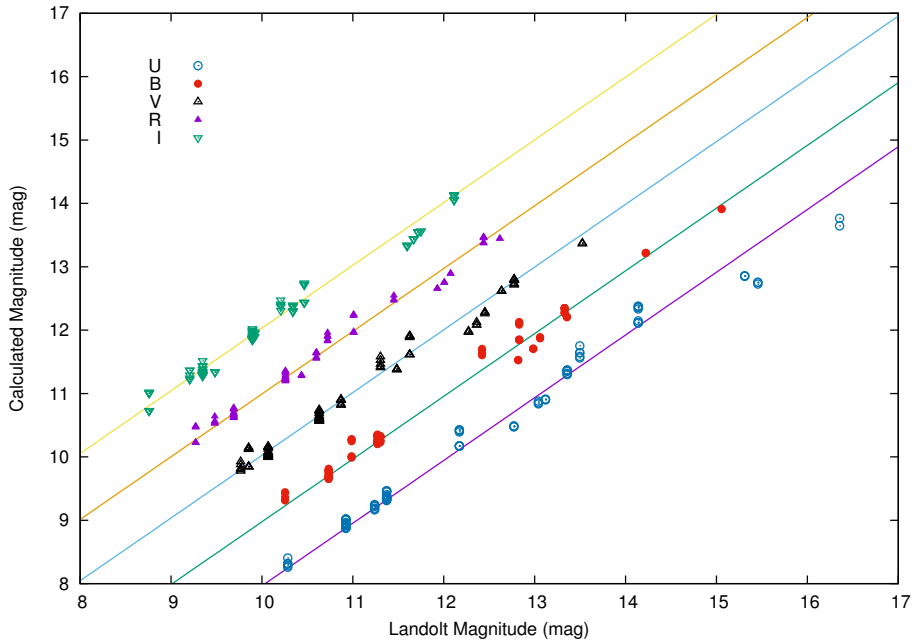

Fig. 6 Landolt magnitudes versus calculated magnitudes using derived transformation coefficients in *UBVRI* bands. The U, B, R, I calculated magnitudes are shifted by $-2, -1, +1, +2$ magnitude, respectively, for clarity. *Solid lines* are the best linear fits.

$N_{\rm dark}$ the dark current per pixel and $N_{\rm readout}$ the readout noise estimated in Section 3.2. The effect of dark current is neglected here. We can easily get the photometric error from the signal-to-noise ratio (SNR) by the equation above, where σ in Equation (10) is the photometric error for objects. 1.0857 is the correction term between an error in electron flux and same error in magnitude.

To check the reliability of the calibration relationship, we carried out observations targeting globular cluster M92 during one night in June 2016. Here, the relations among the exposure time, SNR and star magnitude which we obtained are based on IRAF photometric results. To avoid saturation and get higher SNR, the exposure time was 600 s for U, 160 s for B, 144 s for V, and 72 s for R and I bands. The relationship between the

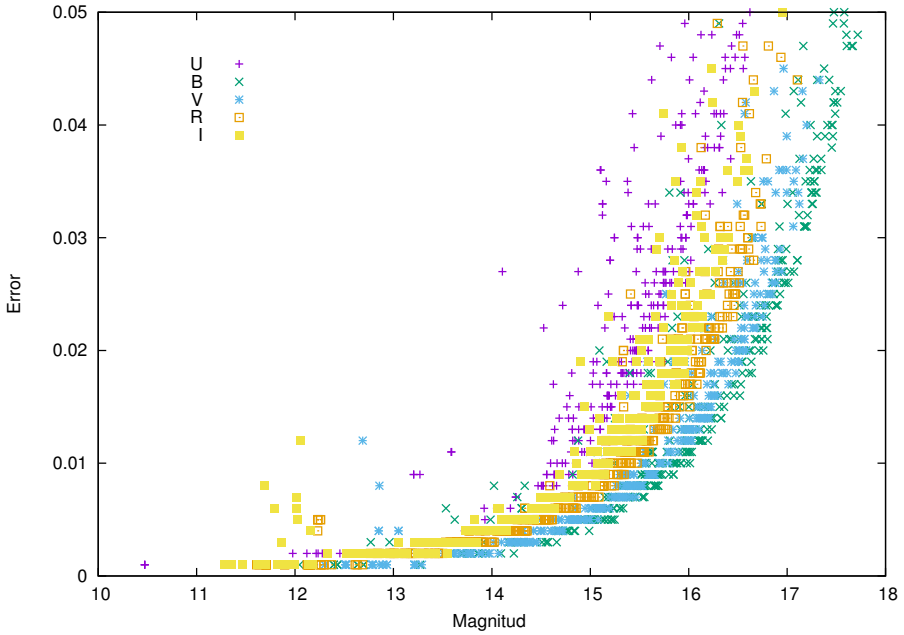

Fig. 7 Photometry error versus calibrated magnitude of M92 with 600 s exposure for U, 160 s exposure for B, 144 s exposure for V, and 72 s exposure for R and I bands.

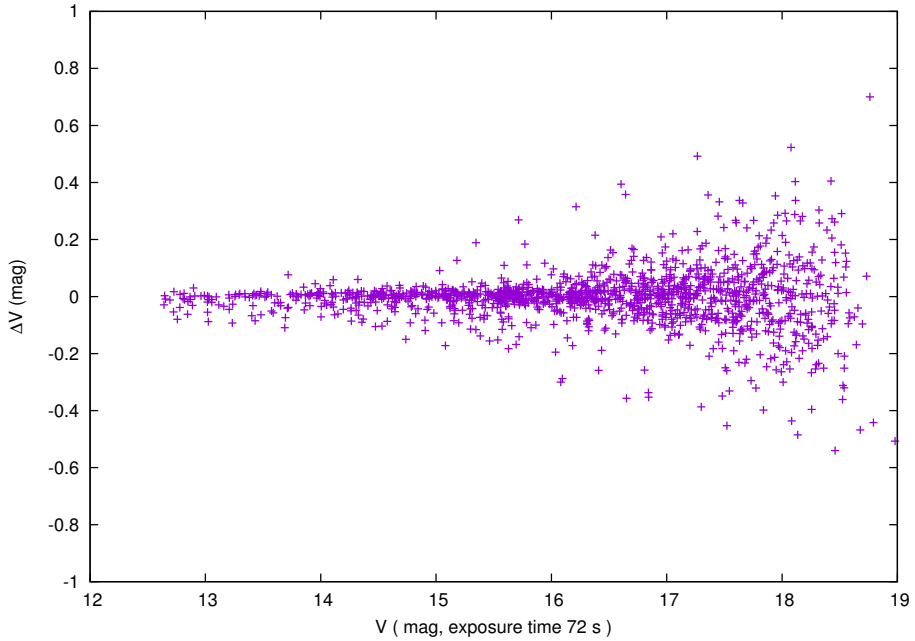

Fig. 8 Photometric accuracy in the V band with exposure time of 72 s.

brightness and photometry error is shown in Figure 7. We took two 72 s exposures of M92, then photometry of all stars with SNR higher than 2 was acquired. The brightness versus photometric accuracy ΔV of corresponding measurements is plotted in Figure 8. It is similar to results from the Weihai Observatory (Hu et al. 2014).

Table 7 The Total Throughput for the 85-cm Telescope in $UBVRI$ Bands

Band	U	B	V	R	I
Throughput	4.5%	23.5%	33.8%	28.2%	27.8%

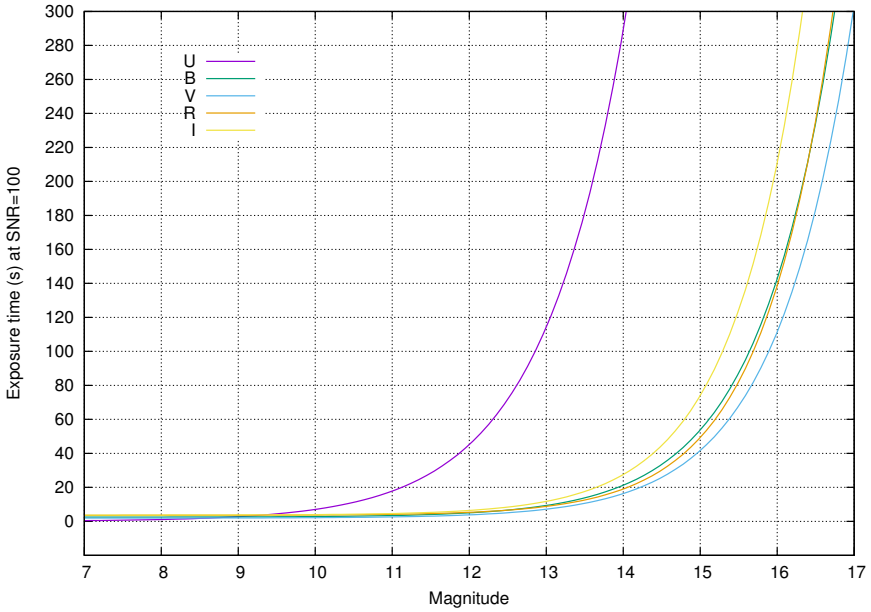

Fig. 9 Exposure time with limiting magnitude at SNR = 100.

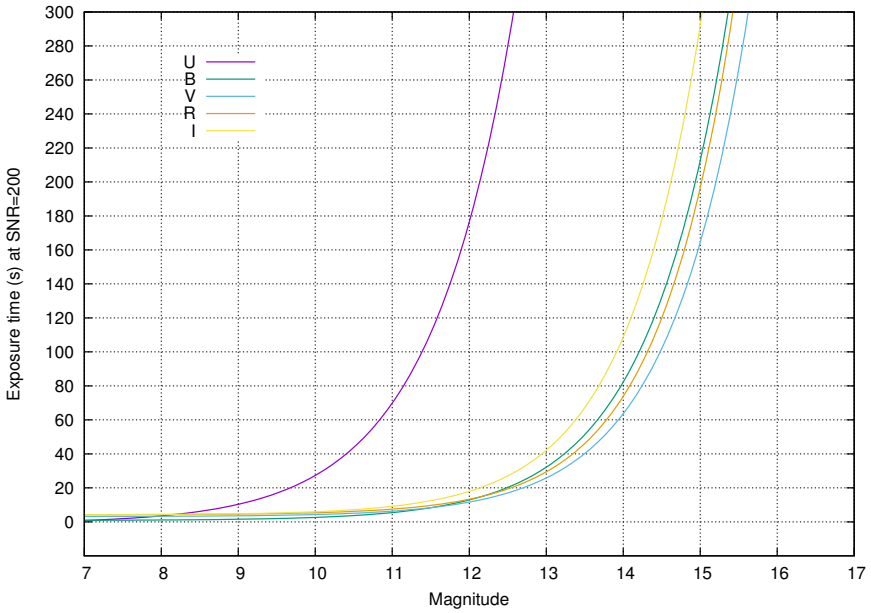

Fig. 10 Exposure time with limiting magnitude at SNR = 200.

During the night the test was conducted, we made five sets of different exposure times in each filter. The airmass was changing during the observations. After the standard reduction, we obtained the time, magnitude and photometric accuracy with different airmasses in each band. So, the relationship between the SNRs of the limiting magnitudes which changed with exposure time and the airmass can be derived.

In Figures 9 and 10, we plot the limiting magnitude with SNR of 100 and 200, respectively, versus the exposure time. Observers can use these figures to estimate the exposure time of their targets. Based on our observations, a simulation was done with a 300 s exposure at the zenith. The limiting magnitudes with SNR of 5 and exposure of 300 s are 18.7, 20.9, 21.1, 20.6 and 20.3 mag in the U, B, V, R and I bands, respectively.

6 SUMMARY

In this paper, we introduce the photometric system of the upgraded 85-cm telescope. In order to offer more valuable information for observers, we test the bias, gain, readout noise, dark current and linearity of the CCD camera which is mounted at the prime focus. The results show that it is a very good scientific-grade camera. Based on several nights of observations using several Landolt standards, the transformation coefficients are derived between the instrumental $UBVRI$ magnitude and the standard magnitude. The atmospheric extinction coefficients and color terms are found to be similar to historical measurements. Due to the new corrector and CCD camera, the throughput of the 85-cm telescope is better than other small size telescopes located at Xinglong station. The limiting magnitude can reach 18.7, 20.9, 21.1, 20.6 and 20.3 mag in the U, B, V, R and I bands respectively with SNR of 5 and exposure of 300 s. Finally, we calculate the limiting magnitude versus the exposure time at different SNRs to give some guidance regarding exposure.

Acknowledgements We gratefully acknowledge support from the staff at the Xinglong 85-cm telescope. JNF acknowledges support from the National Natural Science Foundation of China (NSFC) through grant 11673003 and the National Basic Research Program of China (973 program, 2014CB845700). This work was partially supported by the Open Project Program of the Key Laboratory of Optical Astronomy (National Astronomical Observatories), NSFC under Grant Nos. 11403088 and 11273051 (Xinjiang Astronomical Observatory), Chinese Academy of Sciences and Department of Astronomy, Beijing Normal University.

References

Bohlin, R. C. 2014, AJ, 147, 127
Bohlin, R. C., & Gilliland, R. L. 2004, AJ, 127, 3508
Fan, Z., Wang, H., Jiang, X., et al. 2016, PASP, 128, 115005
Howell, S. B. 2000, Handbook of CCD Astronomy (Cambridge: Cambridge University Press)
Hu, S.-M., Han, S.-H., Guo, D.-F., & Du, J.-J. 2014, RAA (Research in Astronomy and Astrophysics), 14, 719
Huang, F., Li, J.-Z., Wang, X.-F., et al. 2012, RAA (Research in Astronomy and Astrophysics), 12, 1585
Jones, D. 2006, The Observatory, 126, 379
Kinoshita, D., Chen, C.-W., Lin, H.-C., et al. 2005, ChJAA (Chin. J. Astron. Astrophys.), 5, 315
Landolt, A. U. 1992, AJ, 104, 340
Landolt, A. U. 2013, AJ, 146, 131
Luo, Y. P., Zhang, X. B., Deng, L. C., & Han, Z. W. 2012, ApJ, 746, L7
Shi, H.-M., Qiao, Q.-Y., Hu, J.-Y., & Lin, Q. 1998, Chinese Astronomy and Astrophysics, 22, 245
Yang, Y.-G. 2013, RAA (Research in Astronomy and Astrophysics), 13, 1471
Zhang, X. B., Deng, L. C., & Luo, C. Q. 2012, AJ, 144, 141
Zhang, J.-C., Ge, L., Lu, X.-M., et al. 2015a, PASP, 127, 1292
Zhang, L., Pi, Q., Han, X. L., et al. 2015b, New Astron., 38, 50
Zhang, Y.-P., Jiang, M.-D., Zhang, X.-B., et al. 2015c, Chinese Astronomy and Astrophysics, 39, 28
Zhang, L., & Pi, Q. 2015, Planetary Exploration and Science: Recent Results and Advances, eds. S. Jin, N. Haghighipour, & W.-H. Ip (Springer Geophysics), 279
Zhang, J.-C., Fan, Z., Yan, J.-Z., et al. 2016, PASP, 128, 105004
Zhou, A.-Y., Jiang, X.-J., Zhang, Y.-P., & Wei, J.-Y. 2009, RAA (Research in Astronomy and Astrophysics), 9, 349